



Endogenous dual miRNA-triggered dynamic assembly of DNA nanostructures for *in-situ* dual siRNA delivery

Wukun Zhong¹, Lei Huang¹, Yuhong Lin², Chao Xing³ and Chunhua Lu^{1*}

ABSTRACT A theranostic strategy of multiple microRNA (miRNA)-triggered *in-situ* delivery of small interfering RNA (siRNA) can effectively improve the precise therapy of cancer cells. Benefiting from the advantages of programmability, specific molecular recognition, easy functionalization and marked biocompatibility of DNA nanostructures, we designed a three-dimensional (3D) DNA nano-therapeutic platform for dual miRNA-triggered *in-situ* delivery of siRNA. The 3D DNA nanostructure (TY1Y2) was constructed based on the self-assembly of a DNA tetrahedra scaffold, two sets of Y-shaped DNA (Y1 and Y2), and EpCAM-aptamer which functionalized as the ligand molecule for the recognition of specific cancer cells. After being specifically internalized into the targeted cancer cells, TY1Y2 was triggered by two endogenous miRNAs (miR-21 and miR-122), resulting in the generation of strong fluorescence resonance energy transfer fluorescent signal for dual miRNAs imaging. Meanwhile, the therapeutic siRNAs (siSurvivin and siBcl2) could also be *in-situ* generated and released from TY1Y2 through the strand-displacement reactions for the synergistic gene therapy of cancer cells. This 3D DNA nanostructure integrated the specific imaging of endogenous biomarkers and the *in-situ* delivery of therapeutic genes into the multifunctional nanoplatform, revealing the promising applications for the diagnosis and treatment of cancer.

Keywords: DNA tetrahedra, dynamic assembly, miRNA, *in-situ* delivery, cell imaging, gene therapy

INTRODUCTION

Small interfering RNA (siRNA)-based gene therapy can efficiently silence the gene of the relevant disease-causing proteins, thus achieving the purpose of treating the disease [1–3]. Despite the advantages of high specificity and excellent therapeutic efficacy, siRNA has a short half-life and poor biostability, making it difficult to reach the focal tissue site [2–4]. In addition, the non-specific delivery and uncontrollable release of siRNA may induce side effects and systemic toxicity for normal tissues [5,6]. Therefore, it is urgently needed to construct an intelligent siRNA delivery system with high specific targeting ability and *in-situ* controllable release capacity.

In recent years, a variety of functional nanocarriers have been developed for the effective delivery of siRNA, including virus carriers [7], liposomes [8], cationic polymers and inorganic nanomaterials [9]. However, these conventional drug delivery nanocarriers still have certain limitations, such as poor specificity, potential cytotoxicity and unintended release. To compensate the inherent defects of these traditional delivery nanocarriers, DNA nanostructures with great physicochemical properties and marked biocompatibility offer alternative strategies to achieve intelligent gene delivery [5,10–14]. Currently, many DNA nanostructure-based delivery systems have been developed and attracted wide interests. For example, DNA tetrahedron is a classical three-dimensional (3D) scaffold structure with the advantages of predictability, structural stability and remarkable transmembrane performance. Besides, the DNA tetrahedron modified with specific targeting ligands can significantly improve its recognition ability and enhance the cellular uptake efficiency of gene drugs, minimizing the off-target effects for systemic toxicity [15,16]. Lin's group [17] designed a DNA tetrahedron modified with the AS1411 aptamer (a DNA aptamer targeting the nucleolin receptor on the surface of cancer cells) for specific targeted delivery of siRNA into certain cancer cells. However, the *in-vitro* pre-assembled siRNA may induce the decreased therapeutic effect of siRNA due to their unsatisfied biostability and uncontrollable directional release [5,6]. Under these circumstances, many efforts have been made to realize the stimuli-responsive release of siRNA by endogenous substances, such as pH [18], adenosine triphosphate (ATP) [19], reactive oxygen species (ROS) [20] and glutathione (GSH) [14]. Nevertheless, many stimulatory molecules are commonly expressed in normal cells, and the large differences in physicochemical properties of DNA nanostructures also tend to reduce the precision of siRNA delivery. Thus, it is necessary to construct an intelligent nanocarrier that can specifically deliver siRNA into certain cancer cells with high precision and realize the controllable release of siRNA for gene therapy.

Among numerous endogenous stimuli, the abnormal expression of microRNA (miRNA) inside cells is closely related to the occurrence and development of cancers [21–24]. Therefore, the aberrant miRNA can act as an important kind of biomarkers for early cancer diagnosis, and it can also be employed as an endogenous stimulus to trigger the controllable release of ther-

¹ MOE Key Laboratory for Analytical Science of Food Safety and Biology, Fujian Provincial Key Laboratory of Analysis and Detection Technology for Food Safety, State Key Laboratory of Photocatalysis on Energy and Environment, College of Chemistry, Fuzhou University, Fuzhou 350116, China

² Institute of Nanobiomaterials and Immunology, School of Life Science, Taizhou University, Taizhou 318000, China

³ Fujian Key Laboratory of Functional Marine Sensing Materials, Center for Advanced Marine Materials and Smart Sensors, Minjiang University, Fuzhou 350108, China

* Corresponding author (email: chunhualu@fzu.edu.cn)

apeutic genes [23–25]. In addition, miRNA-triggered *in-situ* assembly of siRNA brings more significant specificity, which effectively reduces the accidental leakage of siRNA [26]. Despite the advantages of miRNA-triggered gene release, single-targeted miRNA-based stimuli-response may cause “false positive” results [26,27]. The *in-situ* siRNA assembly with multi-miRNAs as specific triggers can significantly improve the precise intracellular delivery of siRNA with maximum decreased non-specific accumulation.

Herein, we developed a novel theranostic DNA nanostructure that enabled the specific imaging of cancer-relevant miRNAs and *in-situ* siRNA assembly based on dual miRNA-triggered “AND” gate logic operations. The DNA nanostructure (TY1Y2) was self-assembled by a EpCAM aptamer-functionalized DNA tetrahedron (Apt-SDT) and two Y-shaped nucleic acid units (Y1 and Y2), in which miRNA recognition sequences and functional

siRNA sequences were allocated and recombined to construct a pair of “two in one” Y-shaped nucleic acids (Fig. 1). The EpCAM aptamer on TY1Y2 could specifically target and bind to the epithelial cell adhesion molecules that are over-expressed on the cancer cell membrane [28]. Meanwhile, Cy3 and Cy5 fluorescent molecules were modified to achieve the miRNA-triggered specific cell imaging. After being specifically internalized by cancer cells, the dynamic DNA strand-displacement reaction of Y-shaped nucleic acids on TY1Y2 was initiated in the presence of over-expressed miR-21 and miR-122, resulting in the strong fluorescence resonance energy transfer (FRET) inside cancer cells. Additionally, the *in-situ* intracellular generation of siRNAs against Survivin and Bcl2 (siSurvivin and siBcl2, respectively) was accomplished. It was well demonstrated that TY1Y2 enabled specific miR-21/122-triggered cell imaging and intracellular siRNA assembly for effective synergistic gene silencing, which

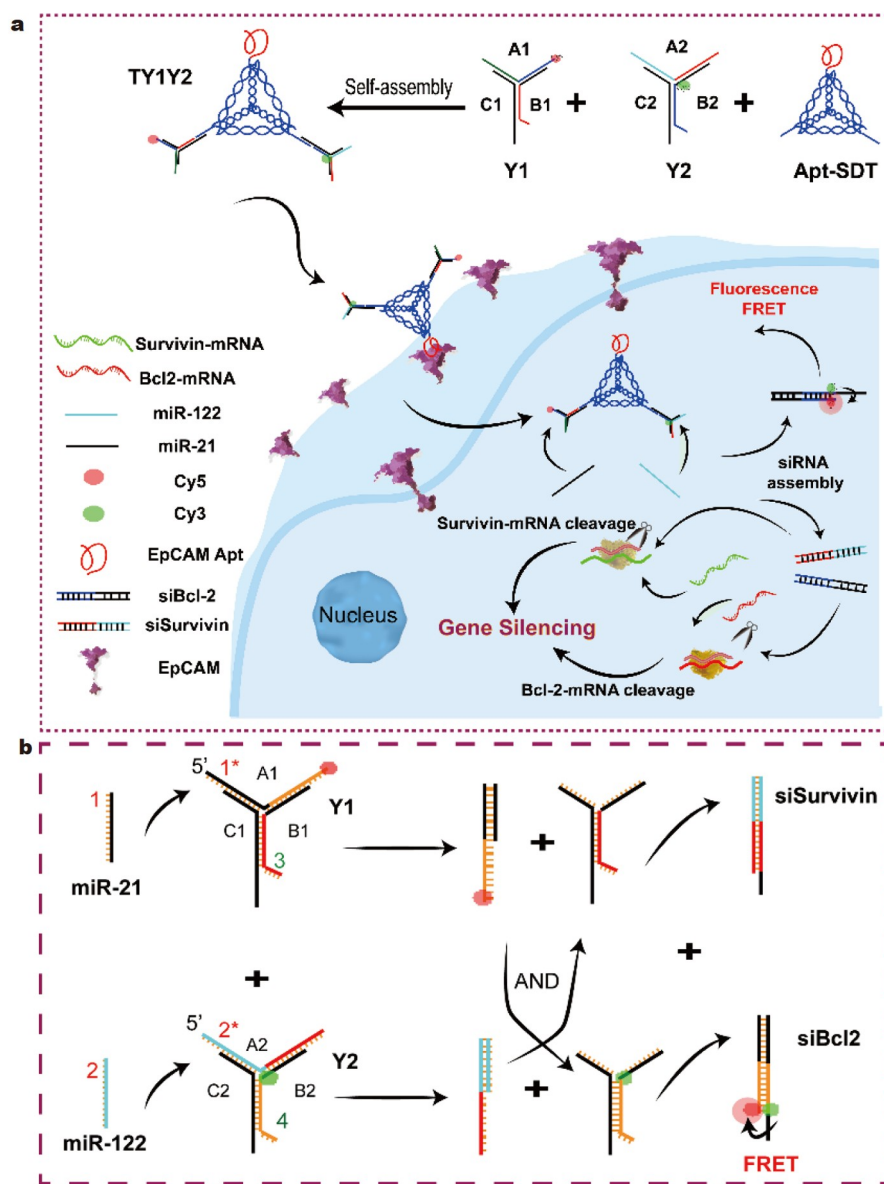


Figure 1 (a) Schematic diagram of TY1Y2 nanostructure for specific cancer diagnosis and treatment. (b) Recovery of FRET fluorescence triggered by dual-miRNA and the dynamic assembly process between Y1 and Y2 in the presence of miR-21 and miR-122.

induced the apoptosis of cancer cells by down-regulating the expression levels of Survivin and Bcl2 proteins.

EXPERIMENTAL SECTION

Materials

GelRed nucleic acid dye was purchased from Liji Biotechnology Co., Ltd. (Shanghai, China). Acrylamide/methanediylbisacrylamide solution (29:1), 1× TAE (Tris-acetate-ethylene diamine tetraacetic acid (EDTA)) buffer and 5× TBE (Tris-borate-EDTA) buffer were purchased from Biotech Bioengineering Co., Ltd. (Shanghai, China). All RNA and DNA sequences were synthesized and purified (HPLC) by Sangon Biotechnology Co., Ltd. (Shanghai, China), and the corresponding nucleic acid sequences were listed in Table S1. Dulbecco's modified Eagle's medium (DMEM), fetal bovine serum (FBS), penicillin/streptomycin and phosphate buffer (PBS) were obtained from Hyclone (U.S.A). Annexin V-fluorescein isothiocyanate (FITC) apoptosis assay kit was from Biotechnology Co., Ltd. (Shanghai, China). Anti-Survivin antibody was purchased from Abcam (UK). Anti-Bcl2 antibody was purchased from Hua'an Bio (Hangzhou, China). Anti-actin antibody and horseradish peroxidase (HRP)-labeled secondary antibody were purchased from Cell Signaling Technology (USA). TransZol Up Plus RNA Kit, TransScript® One-Step gDNA Removal and cDNA Synthesis SuperMix (AT311) and PerfectStart® Green qPCR SuperMix (AQ601) were purchased from TransGen Biotech (Beijing, China). All solutions were prepared by using ultrapure water (18.2 MΩ cm resistivity, Milli-Q, Millipore).

Characterization

The fluorescent intensity was measured by using a fluorescence spectrophotometer (Agilent Technologies, USA). Ultraviolet-visible (UV-vis) absorption spectra were acquired by an SH-1000 microplate reader (Hitachi, Japan). Images of gel electrophoresis were acquired by a ChemiDoc™ Touch gel imager (Bio-Rad, USA). Hydrodynamic diameters were measured by using a Malvern laser particle size meter (Malvern Instruments Ltd., UK). Atomic force microscopy (AFM) images were obtained by a Mult Mode 8 atomic force microscope (Bruker, Germany). Fluorescent images were obtained by a confocal microscope (Nikon, Japan). The apoptosis assay was determined by a CytoFLEX flow cytometer (Beckman, USA).

Preparation of Y-shaped nucleic acids and DNA tetrahedron

Both Y-shaped nucleic acids (Y1 and Y2) and the DNA tetrahedron (Apt-SDT) were formed by one-step annealing self-assembly. Y1 and Y2 were assembled by respectively mixing the corresponding nucleic acid strands (A1, B1 and C1; A2, B2 and C2) with equimolar concentrations in 1× TAE buffer containing 12.5 mmol L⁻¹ MgCl₂. The mixtures were annealed at 95°C for 5 min, and then slowly cooled to room temperature. The Apt-SDT was prepared by mixing S1, S2, S3-EpCAM and S4 at equimolar concentrations in the same way.

Preparation of TY1Y2

Y1, Y2 and Apt-SDT were mixed at equimolar concentrations in 1× TAE buffer containing 12.5 mmol L⁻¹ MgCl₂, and the hybridization reaction was thermostatically performed at 25°C for 2 h to assemble TY1Y2 nanostructure. The successful assembly of Y1, Y2, Apt-SDT and TY1Y2 was verified by 3%

agarose gel electrophoresis, and the images were acquired by the gel imager.

Logical response of Y-shaped nucleic acids

Y1 and Y2 were mixed with miR-21, miR-122 and miR-21/122 samples (where miR-21/122 indicated the mixture of miR-21 and miR-122 with the same concentration) at 30°C for 1 h, respectively. The logical response behavior of Y-shaped nucleic acids to miR-21/122 was proved by 16% polyacrylamide gel electrophoresis (PAGE).

Fluorescence characterization

First, TY1Y2 (100 nmol L⁻¹) was mixed with equimolar concentrations of miR-21, miR-122 and miR-21/122, respectively. After the mixtures were incubated at 30°C for 1 h, the fluorescence spectra of FRET were collected ($\lambda_{\text{ex}} = 530 \text{ nm}$, $\lambda_{\text{em}} = 550\text{--}750 \text{ nm}$).

Meanwhile, kinetic fluorescence tests of TY1Y2 were also performed. TY1Y2 (100 nmol L⁻¹) was mixed with equimolar concentrations of miR-21/122, and the fluorescence change curves were obtained ($\lambda_{\text{ex}} = 530 \text{ nm}$, $\lambda_{\text{em}} = 667 \text{ nm}$). Then, the response behavior of TY1Y2 in the presence of different concentrations of targeted miRNA was verified. TY1Y2 (100 nmol L⁻¹) was mixed with different concentrations of miR-21/122 (0, 10, 20, 30, 50, 75, 100 and 125 nmol L⁻¹, respectively). After incubation at 30°C for 1 h, the fluorescence intensity spectra of FRET were collected. In addition, for demonstrating the selectivity of TY1Y2, TY1Y2 (100 nmol L⁻¹) was mixed with miR-21/miR-122, miR-21/miR-122-m1 (single-base mismatch), miR-21/miR-122-m3 (triple-base mismatch) and miR-21/miR-155 (random sequence) at 30°C for 1 h, respectively. The fluorescence intensity spectra of FRET were recorded.

The stability characterization of TY1Y2

The stability of TY1Y2 in 10% FBS was firstly verified. TY1Y2 (250 nmol L⁻¹) was incubated in 10% FBS solution at 37°C for various time intervals (0, 4, 8, 12 and 24 h, respectively). The concentration changes of TY1Y2 were qualitatively analyzed by 3% agarose gel electrophoresis, and the FRET fluorescence changes of TY1Y2 were collected by fluorescence spectra. For validating the anti-enzymatic digestion capacity of TY1Y2, TY1Y2 (250 nmol L⁻¹) was mixed with 0.5 U mL⁻¹ DNase I and incubated at 37°C for 0, 15, 30, 45 and 60 min, respectively. The stability of TY1Y2 was analyzed by 3% agarose gel electrophoresis. Furthermore, the stability of TY1Y2 in cell lysates was also tested. Briefly, Huh-7 cells (1 × 10⁶) were digested with trypsin and then resuspended in pre-chilled lysis buffer. The mixture was centrifuged (12,000 r min⁻¹) at 4°C for 5 min and the supernatant was stored at -20°C. Subsequently, Y1, Y2 and TY1Y2 were mixed with fresh Huh-7 cell lysate and incubated at 37°C for 0, 4, 8, 12, 24 and 32 h, respectively. The appropriate amounts of mixtures were taken for 3% agarose for gel electrophoresis analysis.

Cell lines

All cell lines were purchased from ATCC. Human hepatocellular carcinoma cell line (Huh-7 cells) was used as the target cell model and cultured with DMEM medium (Hyclone, USA). Human embryonic kidney cell line (HEK293T cells) and human cervical cancer cell line (Hela cells) were used as control cell lines and cultured with MEM medium (Hyclone, USA). Both cell

culture media contained 10% FBS and 100 IU mL⁻¹ penicillin/streptomycin. Cells were incubated at 37°C with 5% CO₂.

Confocal microscopy assay

For studying the cellular uptake of TY1Y2, Huh-7 cells (2.5 × 10⁵) were seeded in confocal dishes and incubated at 37°C for 24 h. Cells were washed with PBS and co-incubated with TY1Y2 (150 nmol L⁻¹) at 37°C for 0, 4 and 6 h, respectively. After washing with PBS, FRET fluorescence signals inside the cells were acquired by a confocal microscopy ($\lambda_{\text{ex}} = 543 \text{ nm}$, $\lambda_{\text{em}} = 552\text{--}617 \text{ and } 662\text{--}737 \text{ nm}$). To investigate the intracellular imaging of different levels of miR-21 and miR-122, anti-miR-21/122 and miR-21/122-mimics were pre-transfected into Huh-7 cells by using lipo8000 to achieve differential contents of miR-21/122 in Huh-7 cells. Subsequently, Huh-7 cells were seeded in confocal dishes and incubated for 24 h, and TY1Y2 was co-incubated with Huh-7 cells at 37°C for 6 h. After washing with PBS, FRET fluorescence images were acquired. To verify the specific cell recognition of TY1Y2, Huh-7 cells (with high levels of miR-21 and miR-122), Hela cells (with high level of miR-21 and low level of miR-122) and HEK293T cells (with low levels of miR-21/122) were used to probe the specific recognition of different cell lines. Huh-7 cells, Hela cells and HEK293T cells were co-incubated with TY1Y2 at 37°C for 6 h, respectively, and the FRET fluorescence images were acquired. Additionally, to demonstrate the specific targeting ability of EpCAM aptamer-functionalized TY1Y2, Huh-7 cells were treated with or without EpCAM aptamer-functionalized TY1Y2 (modified Cy3 fluorescent motif only) at 37°C for 6 h, respectively, and confocal fluorescence images were subsequently acquired.

Cell proliferation inhibition assay

The corresponding DNA sequences were replaced with RNA sequences (sense or antisense sequences of siRNA), while sequences were kept consistent and only the de-oxy-ribonucleotides were changed to the corresponding ribonucleotides. Four groups of samples for experimental test were applied: TY1Y2 containing both siBcl2 and siSurvivin sequences (TY1Y2 (siBcl2/siSurvivin)), TY1Y2 containing only siBcl2 sequence (TY1Y2 (siBcl2)), TY1Y2 containing only siSurvivin sequence (TY1Y2 (siSurvivin)) and naked siBcl2/siSurvivin sequences. Huh-7 cells (7 × 10³) were seeded in a 96-well plate and incubated for 24 h. Then, different samples with various concentrations were added and co-incubated with cells at 37°C for 48 h, respectively. After washing with PBS, 10 μL of CCK-8 reagent and 90 μL of culture medium were added into each well, and cells were incubated for another 50 min. Absorption values at 450 nm were detected and the cell viability was calculated.

Western blot assay (WB)

Huh-7 cells (1 × 10⁵ per well) were seeded in a 6-well plate and incubated for 24 h. Naked siRNA, TY1Y2 (siBcl2), TY1Y2 (siSurvivin) and TY1Y2 (siBcl2/siSurvivin) were co-incubated with Huh-7 cells, respectively. After 48 h incubation, cells were lysed with cell lysis buffer containing protease inhibitor and phosphatase inhibitor. The supernatant protein samples were collected by centrifugation at 4°C, and the total protein concentration was quantified using the BCA Protein Quantification Kit. Subsequently, proteins were separated by using sodium dodecyl sulfate (SDS)-polyacrylamide gels. After transferring the band to polyvinylidene fluoride (PVDF) membranes, PVDF

membranes were blocked with 5% skim milk solution for 2 h. Then, corresponding specific antibodies (anti-Survivin, anti-Bcl2 and anti-Actin antibodies) were added separately and incubated at 4°C overnight. The PVDF membranes were washed three times with 1× TBST (TBS + Tween) buffer. HRP-labeled secondary antibody was added and incubated at room temperature for another 1.5 h. Finally, the membranes were washed three times with 1× TBST, and the expression levels of Survivin and Bcl2 were imaged and analyzed by using a chemiluminescence system.

Annexin V-FITC/propidine iodide (PI) apoptosis analysis

Huh-7 cells (1 × 10⁵ per well) were seeded in a 6-well plate and incubated at 37°C for 24 h. Naked siRNA, TY1Y2 (siBcl2), TY1Y2 (siSurvivin) and TY1Y2 (siBcl2/siSurvivin) were co-incubated with Huh-7 cells for 48 h, respectively. After washing with PBS, cells were digested with trypsin, followed by staining with Annexin V-FITC/PI apoptosis detection kit. The apoptosis results were analyzed by flow cytometry.

Quantitative reverse transcriptase polymerase chain reaction (qRT-PCR) experiment

The expression levels of miR-21 and miR-122 in different cell lines were measured by qRT-PCR analysis. Briefly, the total cellular RNA was extracted by TransZol Up plus RNA kit according to the manufacturer's protocol. Then, the corresponding cDNAs were synthesized through TransScript® One-Step gDNA Removal and cDNA Synthesis SuperMix (AT311) according to the instruction. cDNA was diluted five times and qPCR analysis was performed by PerfectStart® Green qPCR SuperMix (AQ601). The total reaction volume was 20 μL , including 2 μL cDNA template, 0.4 μL forward primer (10 $\mu\text{mol L}^{-1}$), 0.4 μL reverse primer (10 $\mu\text{mol L}^{-1}$), 0.4 μL Dye II (50×), 10 μL PerfectStart® Green qPCR SuperMix (2×) and 6.8 μL Nuclease-free Water. U6 was used as the endogenous control gene. The reaction mixture was heated at 94°C for 30 s, followed by 40 cycles of 94°C for 5 s and then 60°C for 30 s. The related primer sequences were listed in Table S2, and the relative expression levels of miRNAs were calculated by using 2^{- $\Delta\Delta\text{CT}$} method.

RESULTS AND DISCUSSION

Construction of TY1Y2

TY1Y2 consisted of an EpCAM aptamer-functionalized DNA tetrahedral scaffold (Apt-SDT) and two Y-shaped nucleic acid units (Y1 and Y2) (Fig. 1). Y1 was assembled by A1, B1 and C1 single-stranded nucleic acids, and Y2 was assembled by A2, B2 and C2 single-stranded nucleic acids, respectively. The antisense and sense sequences of siBcl2 were inserted into B2 (yellow domain) and A1 (yellow domain), and the sense and antisense sequences of siSurvivin were designed in B1 (red domain) and A2 (red domain), respectively. Owing to the specific recognition of EpCAM aptamer, TY1Y2 could be effectively internalized into cancer cells with the over-expression level of the epithelial cell adhesion molecule, which subsequently realized the endogenous miRNA-triggered cell imaging and gene therapy. Briefly, in the presence of both miR-21 and miR-122, Y1 and Y2 were disassembled simultaneously, inducing the reassignment and formation of miR-21/A1/B2 (containing the siBcl2 duplex motif) and miR-122/A2/B1 (containing the siSurvivin duplex motif)

through toehold-mediated strand-displacement reaction. As a result, the double-strand complexes containing siBcl2 and siSurvivin were *in-situ* generated inside cancer cells, and this process could be monitored through fluorescence changes *via* the fluorophore modification. The released siSurvivin and siBcl2 from TY1Y2 induced synergistic gene therapy and inhibited the proliferation of cancer cells.

Preparation and characterization of TY1Y2

Y1, Y2 and Apt-SDT were firstly prepared by the one-step annealing method and characterized by agarose electrophoresis analysis. As shown in Figs S1 and S2, the migration rates were slower with the addition of various single strands, which indicated the successful assembly of Y1 (Fig. S1, lane 7 on the left), Y2 (Fig. S1, lane 7 on the right) and Apt-SDT (Fig. S2, lane 7). On this basis, Y1 and Y2 were then hybridized to the two vertices of Apt-SDT to assemble TY1Y2. Fig. S3 shows that the bands migrated gradually slower with the addition of Y1 and Y2, suggesting the successful construction of TY1Y2 (lane 6). The hydrodynamic diameters of Apt-SDT and the prepared TY1Y2 measured by dynamic light scattering (DLS) analysis were about 10 and 16 nm, respectively (Fig. S4). In addition, AFM images in Fig. S5 revealed the tetrahedral structures of DNA tetrahedron and TY1Y2. These results demonstrated the successful construction of TY1Y2.

Logic-responsive assembly of TY1Y2 in the presence of miR-21/122

To investigate the specific intracellular miRNA-triggered response of TY1Y2, PAGE analysis was firstly used to analyze the strand-displacement reaction between Y1 and Y2 that triggered by miR-21 and miR-122. As shown in Fig. S6, after the

progressive addition of miR-21 and miR-122, the bands of Y1 and Y2 gradual disappeared (lane 5, lane 4 and lane 3, respectively) and the miR-21/A1/B2 and miR-122/A2/B1 duplex structures appeared (lane 2), which indicated the desired strand displacement between Y1 and Y2 in the presence of both miR-21 and miR-122. For further demonstrating the stimuli-responsive property of TY1Y2, Cy5 and Cy3 were labelled on A1 and B2, respectively, and the fluorescence spectrum was acquired to validate the responsive assembly process of TY1Y2. In the presence of both miR-21 and miR-122, the A1 and B2 on TY1Y2 were triggered and formed the stable double-strand complexes. Thus, Cy5 and Cy3 were in close proximity to each other, and the FRET signal occurred. Fig. 2a, b reveal that TY1Y2 exhibited an appreciable FRET signal under miR-21 and miR-122 co-stimulation, and a nearly 6-fold higher signal could be seen compared with TY1Y2 without miR-21/miR-122 treatment. In addition, fluorescent kinetic testing demonstrated that TY1Y2 could achieve a logical response for miR-21 and miR-122 within minutes (Fig. S7). This was due to the fact that with the addition of dual toehold on Y1 and Y2, TY1Y2 could be rapidly triggered by the corresponding miRNA, which induced the effective strand-displacement reaction and the re-assembly. Therefore, it is deduced that TY1Y2 can be applied for the specific detection and imaging of intracellular miRNAs and the *in-situ* stimuli-responsive gene release for cancer treatment under miR-21 and miR-122 co-stimulation.

As a diagnostic nanodevice, TY1Y2 needs to be significantly responsive to different concentrations of targets. Fig. 2c shows that TY1Y2 revealed noticeable miRNA-responsive fluorescence changes in a concentration-dependent manner within the range of 10–125 nmol L⁻¹. Then, to demonstrate the selective behavior of TY1Y2 for specific miRNA response, random miR-155

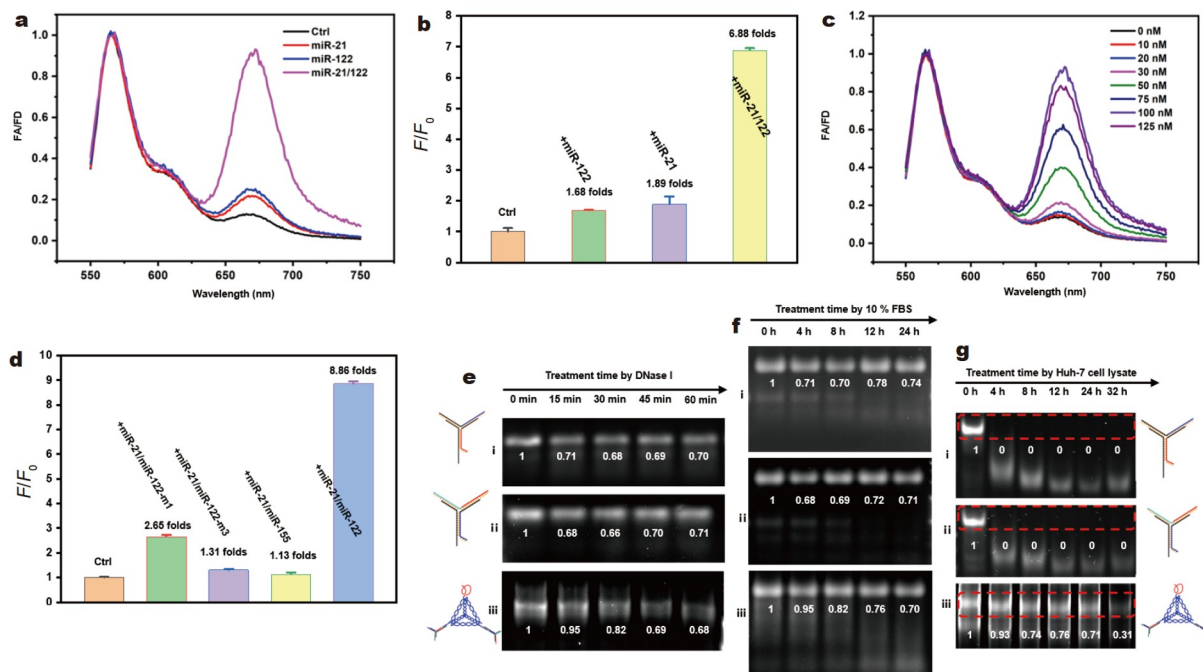


Figure 2 (a) Fluorescence changes and (b) FRET intensity ratios of TY1Y2 in the presence of miR-21, miR-122, and miR-21/miR-122, respectively. FA/FD refers to the fluorescence intensity ratio between Cy5 and Cy3. F/F_0 is the intensity ratio of the FA/FD value of the respective experimental group to the FA/FD value of the blank control group (lacking target miRNA). (c) FRET signal changes with different concentrations of miR-21/miR-122. (d) Specificity of TY1Y2 for various miRNAs. The excitation wavelength was 530 nm and the emission wavelength was 550–750 nm, respectively. (e–g) Gel electrophoresis analysis of the stability of the Y-shaped nucleic acids and TY1Y2 co-incubated with (e) 0.5 U mL⁻¹ DNase I, (f) 10% FBS and (g) cell lysate, respectively.

sequence, miR-122 single-base and triple-base mismatch sequences were chosen for verification. As shown in Fig. 2d, only the exact matching sequences of miR-21 and miR-122 could trigger the re-assembly of TY1Y2 and generate the FRET fluorescent signal. These results suggest that TY1Y2 could achieve the dual-specific recognition of the endogenous miR-21 and miR-122, which provides a promising opportunity for intracellular *in-situ* cell imaging and gene therapy.

Analysis of the stability of TY1Y2

The biological stability of nanomaterials is a prerequisite for applications in biological and biomedical research. Therefore, the biostability of TY1Y2 in complex physiological environments was investigated. Fig. 2e–g show that TY1Y2 was stable enough in both DNase I, 10% FBS and cell lysate. Meanwhile, it was noted that the free Y-shaped nucleic acid structure was also resistant to DNase I and FBS because of its structural rigidity. However, it is susceptible to degradation in the cell lysate. Besides, the fluorescence change of TY1Y2 in 10% FBS solution was also tested. As shown in Fig. S8, no significant fluorescence change of TY1Y2 could be seen after being treated with 10% FBS, further demonstrating the biostability of TY1Y2. Therefore, it is deduced that owing to the rigid structure of the tetrahedral scaffold and the Y-shaped nucleic acid structure, TY1Y2 possesses great biostability to be the nanocarrier for biological applications in living cells.

Analysis of the specific cell recognition and imaging of TY1Y2

To investigate the effective cell uptake of TY1Y2, Huh-7 cells with both high expression levels of miR-21 and miR-122 were employed as the experimental model, and TY1Y2 was co-incubated with Huh-7 cells for various time intervals. Fig. S9 shows that the fluorescence of Cy5 was gradually enhanced with the extended incubation time of TY1Y2, indicating the significant occurrence of FRET effect in the presence of miR-21 and miR-122 inside Huh-7 cells. For further confirming the successful FRET process, acceptor Cy5 was photobleached under the high-power laser irradiation, which resulted in the complete quenching of FRET-induced fluorescence signal and the

enhancement of Cy3 fluorescence (Fig. S10). Therefore, it demonstrated that TY1Y2 could be progressively internalized by Huh-7 cells as the incubation time increased, and TY1Y2 could be effectively stimulated to respond to miR-21 and miR-122 that specifically over-expressed in cancer cells, resulting in the output of FRET fluorescence.

As is known that aptamers are single-stranded oligonucleotides, which can specifically bind to receptors over-expressed on the cancer cell surface to enhance the delivery efficiency and reduce off-target effects of nanocarriers. Therefore, the specific targeting ability of TY1Y2 was investigated. Fig. S11 shows that the fluorescence intensity of Huh-7 cells after being treated with TY1Y2 with EpCAM aptamer modification was significantly higher than that without aptamer modification, which suggested the improved cellular uptake efficiency of TY1Y2 in the presence of EpCAM aptamer. In addition, compared with the obvious strong fluorescent signal in Huh-7 cells, negligible fluorescence could be seen inside HEK293T cells after being incubated with EpCAM aptamer-modified TY1Y2, demonstrating the binding affinity of TY1Y2 against cancer cells (Fig. S12).

Superior diagnostic devices need to output different response signals to cells that expressing differential miRNA levels, which is necessary for the precise diagnosis and treatment of cancer. To evaluate the identification behavior of TY1Y2 for different levels of miRNAs in cancer cells, the miR-21 and miR-122 expression levels in Huh-7 cells were up-regulated and down-regulated by the transfection of miR-21/122 with sense strands mimics and antisense strands mimics, respectively. As shown in Fig. 3, compared with the untreated Huh-7 cells, cells with up-regulated miR-21/122 expression yielded stronger FRET signal, while cells with down-regulated miR-21/122 level presented weaker FRET change. These results indicated that TY1Y2 could distinguish live cells with differential miRNA levels.

Subsequently, whether TY1Y2 could differentiate different cell types with different expressions of miR-21 and miR-122 was also verified. HeLa cells with high expression of miR-21 and negative miR-122 expression, and HEK293T cells with low expression of both miR-21/122 were also used as cell models, respectively [29–31]. Fig. 4 reveals that only Huh-7 cells exhibited a significant

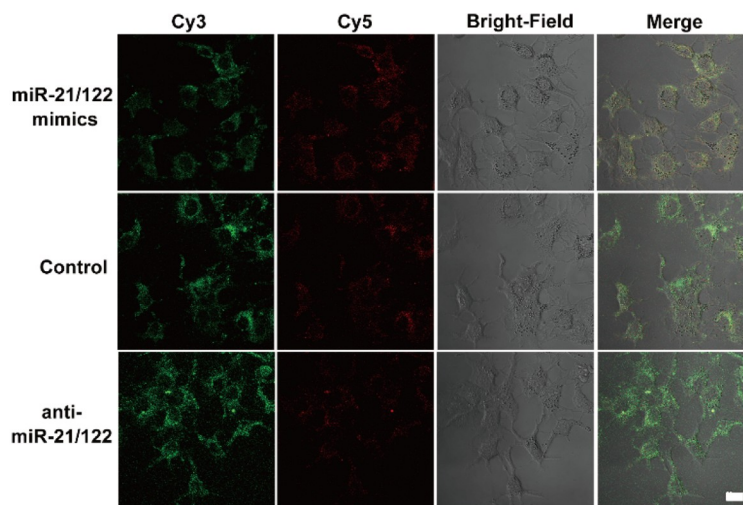


Figure 3 Recognition and imaging behavior of TY1Y2 for Huh-7 cells with different miR-21/122 levels. Huh-7 cells were pretreated with anti-miR-21/122 and miR-21/122 mimics, respectively. The excitation wavelength was 543 nm. The emission wavelengths of Cy3 and Cy5 were 552–617 nm and 662–737 nm, respectively. Scale bar: 20 μ m.

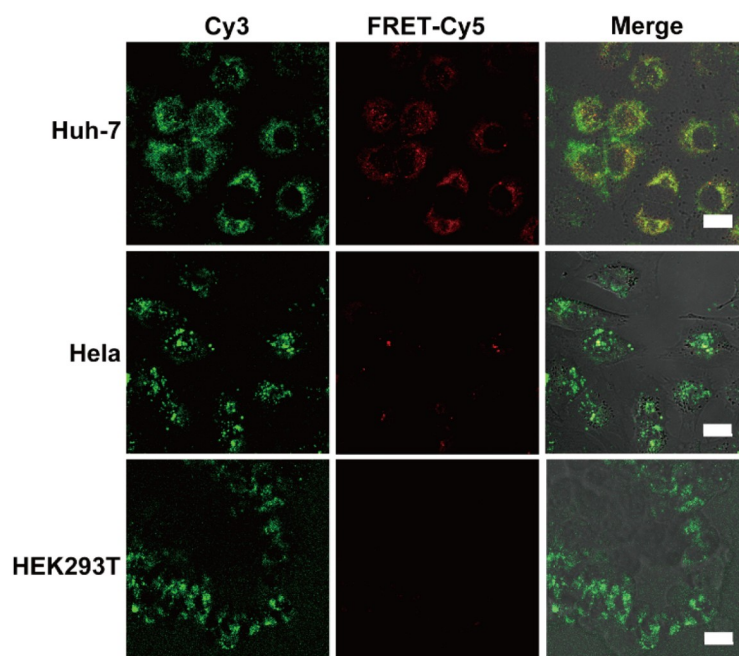


Figure 4 CLSM images of Huh-7 cells, HeLa cells and HEK293T cells after being treated with TY1Y2, respectively. The excitation wavelength was 543 nm. The emission wavelengths of Cy3 and Cy5 were 552–617 nm and 662–737 nm, respectively. Scale bars: 20 μm .

FRET signal. In contrast, the corresponding imaging signal was fragile in both HeLa cells and HEK293T cells, which were consistent with the relative miRNA expression levels in different cell lines that analyzed by qRT-PCR (Fig. S13). These results demonstrated that TY1Y2 could identify and image cancer cells with high miR-21/122 expression and effectively differentiate different cancer cell lines.

***In-vitro* gene therapy effect**

Based on the above experimental studies, TY1Y2 enables both detection and imaging of dual miR-21/122 inside and outside the cells. Thus, it is reasonable to infer that TY1Y2 could realize the *in-situ* generation and release of therapeutic genes by miRNA-responsive strand-displacement reaction in living cells. Prior to investigating the *in-vitro* gene therapy for cancer cells, the biocompatibility of TY1Y2 was first evaluated. The therapeutic siRNA sequences were replaced with the corresponding DNA sequences. As shown in Fig. S14, negligible cell death was observed after cells were co-incubated with TY1Y2 for different times, which suggested the great biocompatibility of the constructed DNA nanoplateform as a drug delivery carrier for the subsequent gene therapy.

Survivin is important for inhibiting apoptosis of cancer cells, which block the activation of the Caspase-dependent signaling pathway by inhibiting the release of cytochrome C from mitochondria [32,33]. Bcl2 is a kind of anti-apoptotic protein that can bind to the pro-apoptotic proteins (BOX and BAD), thus exerting an apoptosis-inhibiting function [34]. Therefore, siSurvivin and siBcl2 were simultaneously used as the two therapeutic genes to realize the synergetic gene therapy in this study. It should be noted that when designing the therapeutic platform for *in-situ* delivery of siRNA, we replaced the corresponding sequences to the RNA sequences, which denoted as TY1Y2(siBcl2/siSurvivin). Subsequently, cytotoxicity by CCK8 assay was studied to evaluate the proliferation inhibition of

TY1Y2(siBcl2/siSurvivin). To verify the synergetic gene therapy, TY1Y2 with only siSurvivin or siBcl2 sequence (TY1Y2(siSurvivin) or TY1Y2(siBcl2)) was employed for comparison. After treatment with different concentrations of the therapeutic platform, the cell proliferation of Huh-7 cells was inhibited in a concentration-dependent manner, while naked siRNA-treated cells showed undesired cell proliferation inhibition (Fig. 5a). It demonstrated that the therapeutic platform could effectively deliver the therapeutic siRNA into targeted cancer cells with high stability compared with the naked siRNA. Additionally, simultaneous delivery of higher concentrations of siBcl2 and siSurvivin had a more pronounced inhibitory effect on cancer cell proliferation, which is attributed to the synergistic gene silencing of the siBcl2 and siSurvivin. Similar results could also be detected by flow cytometry apoptosis analysis (Fig. 5b).

Next, WB was employed to investigate whether TY1Y2(siBcl2/siSurvivin) can down-regulate the related proteins in cancer cells. Fig. 5c shows that the therapeutic platform with different siRNA modifications could effectively regulate the corresponding protein expressions in Huh-7 cells. Among them, TY1Y2 (siBcl2/siSurvivin) effectively down-regulated the expression levels of Bcl2 protein and Survivin protein (lane 5). Meanwhile, TY1Y2(siBcl2) also affected the expression levels of Survivin protein in small amounts (lane3). This is due to the fact that both Survivin and Bcl2 genes are associated with signaling pathways related to cell proliferation and play essential roles in the proliferation of cancer cells. Bcl2 protein over-expressed in cancer cells effectively inhibits the activation of Caspase-3 for cell apoptosis. When Bcl2 protein is down-regulated, the pro-apoptotic proteins BOX and BAD were activated, which promoted the activation of caspase-dependent signaling pathway and affected the function of Survivin. These results demonstrated that TY1Y2(siBcl2/siSurvivin) could release siSurvivin and siBcl2 *in-situ* in the presence of miR-21 and miR-122, thus silencing the expression levels of apoptosis-related proteins and

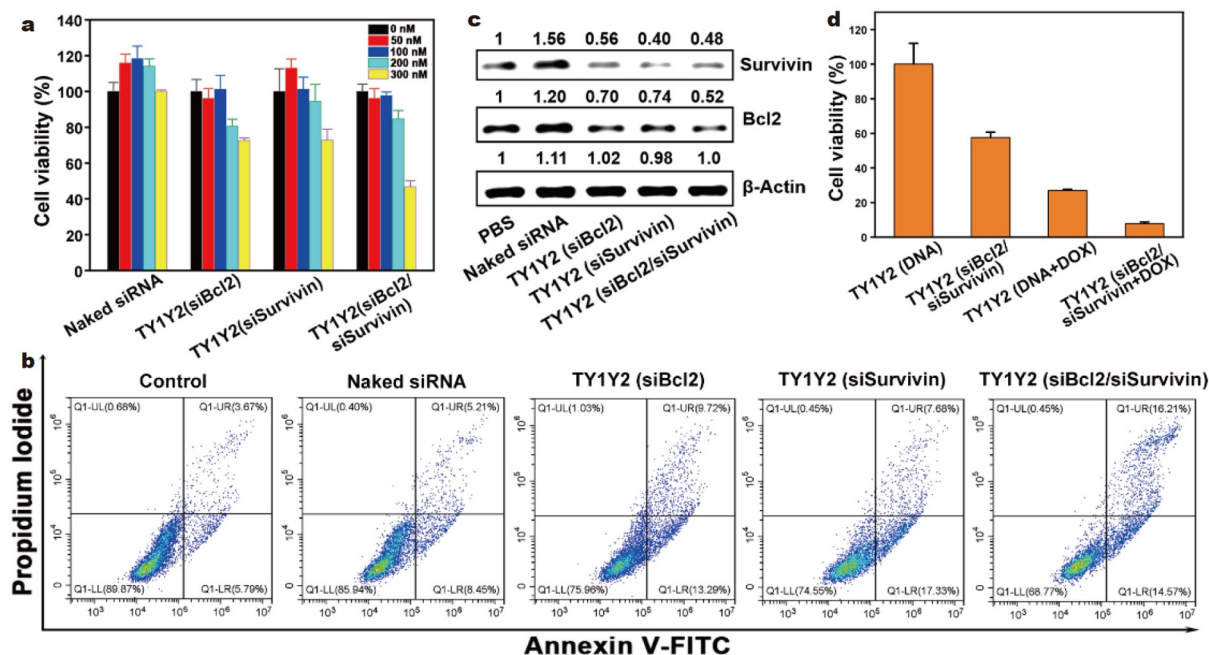


Figure 5 (a) Cell viabilities of Huh-7 cells after incubation with the naked siRNA, TY1Y2 (siBcl2), TY1Y2 (siSurvivin) and TY1Y2 (siBcl2/siSurvivin), respectively. (b) Apoptosis of Huh-7 cells after incubation with the naked siRNA, TY1Y2 (siBcl2), TY1Y2 (siSurvivin) and TY1Y2 (siBcl2/siSurvivin), respectively, and analyzed by flow cytometry. (c) WB analysis of the expressions of Survivin and Bcl2 in Huh-7 cells after different treatments. (d) Cytotoxicity analysis of the therapeutic effect of DOX-embedded TY1Y2 (siBcl2/siSurvivin).

performing the synergistic gene therapy against cancer cells.

Therapeutic effect of TY1Y2 (siBcl2/siSurvivin) combined with chemotherapy and gene therapy

Generally, gene silencing can down-regulate the expression levels of related proteins. However, the down-regulation of protein level is transient and the expression level starts to recover after 48 h of action. Therefore, gene therapy combined with other therapeutic methods, such as chemotherapy, often leads to better cancer treatment results. Decreasing the expression level of oncogenic proteins can significantly reduce the resistance of cancer cells, and thus improve the therapeutic effects of chemotherapeutic drugs. To further explore the effect of TY1Y2 (siBcl2/siSurvivin) on oncoprotein silencing, doxorubicin (DOX) was used as the chemotherapeutic agent and embedded in the GC base pairs of TY1Y2 (siBcl2/siSurvivin). Fig. 5d shows that TY1Y2 (siBcl2/siSurvivin) combined with siBcl2/siSurvivin and DOX caused apparent cell death of Huh-7 cells, which proved that TY1Y2 (siBcl2/siSurvivin) could significantly enhance the therapeutic effect of chemotherapeutic drugs by down-regulating the expression levels of Survivin and Bcl2 proteins.

CONCLUSIONS

In summary, we constructed a 3D DNA nano-therapeutic platform with great biostability and biocompatibility for dual miRNA-triggered intracellular imaging and *in-situ* delivery of siRNAs. The intra/extracellular research results showed that TY1Y2 could specifically respond to the co-stimulation of miR-21 and miR-122. In addition, the modification of EpCAM-aptamer enhanced the specific targeting ability and uptake efficiency of TY1Y2, which finally promoted the effective synergistic gene silencing by *in-situ* assembly of siSurvivin and siBcl2 in the

presence of miR-21 and 122 that are over-expressed in certain cancer cells. Moreover, based on the programmability of nucleic acids and the principle of base complementary pairing, the theranostic TY1Y2 can be used for the identification and specific response of other kinds of biomarkers only by a simple replacement of the corresponding miRNA recognition sequences and siRNA sequences. Benefiting from the great designability, versatility, specificity and biocompatibility of the 3D DNA nano-structure, more programmable nano-diagnosis and treatment platforms can be designed to respond to the specific endogenous biomarkers, which represent a promising opportunity for the precious cancer therapy.

Received 18 November 2022; accepted 6 February 2023;
published online 28 April 2023

- Bumcrot D, Manoharan M, Kotliansky V, *et al.* RNAi therapeutics: A potential new class of pharmaceutical drugs. *Nat Chem Biol*, 2006, 2: 711–719
- Setten RL, Rossi JJ, Han S. Author correction: The current state and future directions of RNAi-based therapeutics. *Nat Rev Drug Discov*, 2020, 19: 290
- Shen S, Dean DC, Yu Z, *et al.* Aberrant CDK9 expression within chordoma tissues and the therapeutic potential of a selective CDK9 inhibitor LDC000067. *J Cancer*, 2020, 11: 132–141
- Kim B, Park JH, Sailor MJ. Rekindling RNAi therapy: Materials design requirements for *in vivo* siRNA delivery. *Adv Mater*, 2019, 31: 1903637
- Jiang Q, Yue S, Yu K, *et al.* Endogenous microRNA triggered enzyme-free DNA logic self-assembly for amplified bioimaging and enhanced gene therapy *via in situ* generation of siRNAs. *J Nanobiotechnol*, 2021, 19: 288
- Hyun S, Choi Y, Lee HN, *et al.* Construction of histidine-containing hydrocarbon stapled cell penetrating peptides for *in vitro* and *in vivo* delivery of siRNAs. *Chem Sci*, 2018, 9: 3820–3827
- Koppers-Lalic D, Hogenboom MM, Middeldorp JM, *et al.* Virus-modified exosomes for targeted RNA delivery; a new approach in na-

- nomedicine. *Adv Drug Deliver Rev*, 2013, 65: 348–356
- 8 Idris A, Davis A, Supramaniam A, *et al.* A SARS-CoV-2 targeted siRNA-nanoparticle therapy for COVID-19. *Mol Ther*, 2021, 29: 2219–2226
 - 9 He X, Yin F, Wang D, *et al.* AIE featured inorganic-organic core@shell nanoparticles for high-efficiency siRNA delivery and real-time monitoring. *Nano Lett*, 2019, 19: 2272–2279
 - 10 Lin S, Xie P, Luo M, *et al.* Efficiency against multidrug resistance by co-delivery of doxorubicin and curcumin with a legumain-sensitive nanocarrier. *Nano Res*, 2018, 11: 3619–3635
 - 11 Gong X, Li R, Wang J, *et al.* A smart theranostic nanocapsule for spatiotemporally programmable photo-gene therapy. *Angew Chem Int Ed*, 2020, 59: 21648–21655
 - 12 Li D, Li X, Yang F, *et al.* Targeted delivery of DNA framework-encapsulated native therapeutic protein into cancer cells. *ACS Appl Mater Interfaces*, 2020, 12: 54489–54496
 - 13 Dong Y, Yao C, Zhu Y, *et al.* DNA functional materials assembled from branched DNA: Design, synthesis, and applications. *Chem Rev*, 2020, 120: 9420–9481
 - 14 Wang Z, Song L, Liu Q, *et al.* A tubular DNA nanodevice as a siRNA/chemo-drug co-delivery vehicle for combined cancer therapy. *Angew Chem Int Ed*, 2021, 60: 2594–2598
 - 15 Mou Q, Ma Y, Ding F, *et al.* Two-in-one chemogene assembled from drug-integrated antisense oligonucleotides to reverse chemoresistance. *J Am Chem Soc*, 2019, 141: 6955–6966
 - 16 Pang L, Shah H, Wang H, *et al.* EpCAM-targeted 3WJ RNA nanoparticle harboring delta-5-desaturase siRNA inhibited lung tumor formation via DGLA peroxidation. *Mol Ther Nucleic Acids*, 2020, 22: 222–235
 - 17 Xiao D, Li Y, Tian T, *et al.* Tetrahedral framework nucleic acids loaded with aptamer AS1411 for siRNA delivery and gene silencing in malignant melanoma. *ACS Appl Mater Interfaces*, 2021, 13: 6109–6118
 - 18 Li C, Zhou J, Wu Y, *et al.* Core role of hydrophobic core of polymeric nanomicelle in endosomal escape of siRNA. *Nano Lett*, 2021, 21: 3680–3689
 - 19 Moore GWK, Howell SEL, Brady M, *et al.* Anomalous collapses of nares strait ice arches leads to enhanced export of arctic sea ice. *Nat Commun*, 2021, 12: 1
 - 20 Chen L, Li G, Wang X, *et al.* Spherical nucleic acids for near-infrared light-responsive self-delivery of small-interfering RNA and antisense oligonucleotide. *ACS Nano*, 2021, 15: 11929–11939
 - 21 Daugaard I, Hansen TB. Biogenesis and function of Ago-associated RNAs. *Trends Genet*, 2017, 33: 208–219
 - 22 Farh KKH, Grimson A, Jan C, *et al.* The widespread impact of mammalian microRNAs on mRNA repression and evolution. *Science*, 2005, 310: 1817–1821
 - 23 Hill M, Tran N. Global miRNA to miRNA interactions: Impacts for miR-21. *Trends Cell Biol*, 2021, 31: 3–5
 - 24 Tavakolizadeh J, Roshanaei K, Salmaninejad A, *et al.* MicroRNAs and exosomes in depression: Potential diagnostic biomarkers. *J Cell Biochem*, 2018, 119: 3783–3797
 - 25 Ren K, Zhang Y, Zhang X, *et al.* *In situ* siRNA assembly in living cells for gene therapy with microRNA triggered cascade reactions templated by nucleic acids. *ACS Nano*, 2018, 12: 10797–10806
 - 26 Yue R, Chen M, Ma N. Dual microRNA-triggered drug release system for combined chemotherapy and gene therapy with logic operation. *ACS Appl Mater Interfaces*, 2020, 12: 32493–32502
 - 27 Keller L, Pantel K. Unravelling tumour heterogeneity by single-cell profiling of circulating tumour cells. *Nat Rev Cancer*, 2019, 19: 553–567
 - 28 Chen X, Chen T, Zhang L, *et al.* Cyclodextrin-mediated formation of porous RNA nanospheres and their application in synergistic targeted therapeutics of hepatocellular carcinoma. *Biomaterials*, 2020, 261: 120304
 - 29 Hemphill J, Deiters A. DNA computation in mammalian cells: MicroRNA logic operations. *J Am Chem Soc*, 2013, 135: 10512–10518
 - 30 Quan K, Li J, Wang J, *et al.* Dual-microRNA-controlled double-amplified cascaded logic DNA circuits for accurate discrimination of cell subtypes. *Chem Sci*, 2019, 10: 1442–1449
 - 31 Liu L, Li N, Huang ZM, *et al.* Gold nanoflares with computing function

as smart diagnostic automata for multi-miRNA patterns in living cells. *Anal Chem*, 2020, 92: 10925–10929

- 32 Martínez-García D, Manero-Rupérez N, Quesada R, *et al.* Therapeutic strategies involving survivin inhibition in cancer. *Med Res Rev*, 2019, 39: 887–909
- 33 Mesri M, Wall NR, Li J, *et al.* Cancer gene therapy using a survivin mutant adenovirus. *J Clin Invest*, 2001, 108: 981–990
- 34 Perini GF, Ribeiro GN, Pinto Neto JV, *et al.* BCL-2 as therapeutic target for hematological malignancies. *J Hematol Oncol*, 2018, 11: 65

Acknowledgements This work was supported by the National Key R&D Program of China (2018YFA0902600), the National Natural Science Foundation of China (22174019), the Natural Science Foundation of Fujian (2020J06036), and Fuzhou Science and Technology Innovation and Entrepreneurial Talent Cultivation Program Project (2022-R-002).

Author contributions Lu C designed the study; Zhong W and Huang L searched the literature and performed the experiments; Lu C, Zhong W and Lin Y analyzed the data; Zhong W, Lin Y and Xing C organized the figures; Zhong W and Lin Y wrote the manuscript with support from Lu C. All authors contributed to the general discussion.

Conflict of interest The authors declare that they have no conflict of interest.

Supplementary information Supporting data are available in the online version of the paper.



Wukun Zhong received his Bachelor's degree (2019) and Master's degree (2022) from the College of Chemistry at Fuzhou University (China). His research focuses on the construction of functionalized DNA nanostructures and nano-diagnosis.



Chunhua Lu received his BS (2005) and PhD (2011) degrees from the College of Chemistry and Chemical Engineering at Fuzhou University (China). From 2011 to 2015, he did his postdoctoral research at The Hebrew University of Jerusalem (Israel) with Prof. Itamar Willner. Dr. Chunhua Lu is currently a professor at the College of Chemistry at Fuzhou University (China). His research interests address topics of DNA nanotechnology, nanobiosensor and chemical biology.

内源性双miRNA触发响应的DNA纳米结构动态自组装用于原位递送siRNA

钟武坤¹, 黄蕾¹, 林玉红², 邢超³, 卢春华^{1*}

摘要 通过多重miRNA触发的原位siRNA递送治疗策略可以有效提高对癌细胞的精确治疗。基于DNA纳米结构的可编程性、特异性分子识别、易于功能化修饰和良好生物相容性的特点,我们设计了一个3D DNA纳米治疗平台,用于实现双miRNA触发响应的siRNA原位递送。这种3D DNA纳米结构(TY1Y2)是由DNA四面体支架、两组Y型DNA(Y1和Y2)和EpCAM核酸适体通过自组装构建而成的。TY1Y2被特异性内化至靶标癌细胞后,能够被两个内源性miRNA(miR-21和miR-122)触发,从而产生强的荧光共振能量转移信号,用于双miRNAs成像。同时,治疗性的siRNA(siSurvivin和siBcl2)也可以通过链置换反应从TY1Y2中产生并进行原位释放,实现癌细胞的协同基因治疗。这种3D DNA纳米结构将内源性生物标记物的特异性成像和治疗性基因的原位递送整合为一个多功能纳米平台,在癌症诊断和治疗方面显示出广阔的应用前景。